AIP | The Journal of Chemical Physics

Initial state resolved electronic spectroscopy of HNCO: Stimulated Raman preparation of initial states and laser induced fluorescence detection of photofragments

Steven S. Brown, H. Laine Berghout, and F. Fleming Crim

Citation: The Journal of Chemical Physics **107**, 8985 (1997); doi: 10.1063/1.475190
View online: http://dx.doi.org/10.1063/1.475190
View Table of Contents: http://scitation.aip.org/content/aip/journal/jcp/107/21?ver=pdfcov
Published by the AIP Publishing

Articles you may be interested in

Analysis and prediction of absorption band shapes, fluorescence band shapes, resonance Raman intensities, and excitation profiles using the time-dependent theory of electronic spectroscopy
J. Chem. Phys. **127**, 164319 (2007); 10.1063/1.2770706

Observation of a new phosphorus-containing reactive intermediate: Electronic spectroscopy and excited-state dynamics of the HPBr free radical
J. Chem. Phys. **123**, 144304 (2005); 10.1063/1.2055227

Twisted intramolecular charge transfer states: Rotationally resolved fluorescence excitation spectra of 4, 4′-dimethylaminobenzonitrile in a molecular beam
J. Chem. Phys. **122**, 084309 (2005); 10.1063/1.1850092

Dissociation dynamics of thiolactic acid at 193 nm: Detection of the nascent OH product by laser-induced fluorescence
J. Chem. Phys. **120**, 6964 (2004); 10.1063/1.1667878

Rotational coherence spectroscopy of para-cyclohexylaniline by stimulated Raman-induced fluorescence depletion and stimulated emission pumping
J. Chem. Phys. **113**, 7830 (2000); 10.1063/1.1314375

This article is copyrighted as indicated in the article. Reuse of AIP content is subject to the terms at: http://scitation.aip.org/termsconditions. Downloaded to IP: 129.174.21.5 On: Wed, 24 Dec 2014 07:00:50

Initial state resolved electronic spectroscopy of HNCO: Stimulated Raman preparation of initial states and laser induced fluorescence detection of photofragments

Steven S. Brown, H. Laine Berghout, and F. Fleming Crim
Department of Chemistry, University of Wisconsin-Madison, Madison, Wisconsin 53706

(Received 22 July 1997; accepted 19 August 1997)

Stimulated Raman excitation (SRE) efficiently prepares excited vibrational levels in the ground electronic state of isocyanic acid, HNCO. Photofragment yield spectroscopy measures the electronic absorption spectrum out of initially selected states by monitoring laser induced fluorescence (LIF) of either NCO ($X\ ^2\Pi$) or NH ($a\ ^1\Delta$) photofragments. Near threshold, the N–H bond fission is predissociative, and there is well-resolved rotational and vibrational structure in the NCO yield spectra that allows assignment of K_a rotational quantum numbers to previously unidentified vibrational and rotational levels in the ν_1 N–H stretch and ν_3 N–C–O symmetric stretch fundamentals in the ground electronic state of HNCO. The widths of NCO yield resonances depend on the initial vibrational state, illustrating one way in which initial vibrational state selection influences dissociation dynamics. Initial excitation of unperturbed ν_1 (N–H stretch) states leads to diffuse NCO yield spectra compared to excitation of mixed vibrational levels. The higher energy dissociation channel that produces NH ($a\ ^1\Delta$) has coarser structure near its threshold, consistent with a more rapid dissociation, but the resonance widths still depend on the initially selected vibrational state. © *1997 American Institute of Physics.* [S0021-9606(97)01444-X]

I. INTRODUCTION

Double resonance excitation to a dissociative electronic state using an excited vibrational level as the intermediate state is a means of studying fully quantum state resolved photodissociation.[1–5] Recently, we reported the double-resonance photodissociation of isocyanic acid,[6–8] a molecule that has three dissociation pathways that follow ultraviolet excitation to the S_1 ($^1A''$) state,[7,9–12]

$$\mathrm{NH}(a\ ^1\Delta)+\mathrm{CO}(X\ ^1\Sigma^+)\quad D_0=42\,765\ \mathrm{cm}^{-1}, \tag{1}$$

$$\mathrm{HNCO}+h\nu\rightarrow\mathrm{H}(X\ ^2S)+\mathrm{NCO}(X\ ^2\Pi)\quad D_0=38\,380\ \mathrm{cm}^{-1}, \tag{2}$$

$$\mathrm{NH}(X\ ^3\Sigma^-)+\mathrm{CO}(X\ ^1\Sigma^+)\quad D_0=30\,080\ \mathrm{cm}^{-1}. \tag{3}$$

The dissociation of the N–H bond, channel (2), occurs indirectly by a crossing from S_1 to S_0, at least in the region within a few thousand wave numbers of its threshold.[7,10] There is a substantial barrier to N–H bond fission on S_1,[13] and NCO photofragment yield spectra and product state distributions from photodissociation of HNCO in a molecular beam are consistent with barrierless dissociation on S_0.[10] Channel (1) is the spin-allowed dissociation of the C–N bond, and its mechanism has received careful scrutiny. It appears, based on NH ($a\ ^1\Delta$) and CO ($X\ ^1\Sigma^+$) rotational distributions,[11] fragment recoil anisotropies,[14–16] and the observation of vibrational state-specific effects in the photodissociation,[6,8] that channel (1) occurs mainly by direct dissociation on the S_1 surface, which has a small ($\sim$500 cm^{-1}) barrier to C–N bond fission.[7,11,13] Channel (3) is a spin-forbidden process on S_1 and, therefore, must occur via a crossing to the triplet surface (T_1).[15,17] We have not explored the triplet channel in the work described here. The electronic transition to S_1 changes the equilibrium N–C–O angle from its nearly linear ground state geometry[18,19] to a bent excited state configuration,[20–23] as Fig. 1 illustrates. The S_1 state has minima for both *cis* and *trans* isomers,[13,20] although the excitation of the *trans* isomer appears to dominate the electronic excitation spectrum out of the ground vibrational state in S_0.[24]

Isocyanic acid has complex vibrational spectroscopy in addition to rich photochemistry. Using stimulated Raman excitation (SRE) (Ref. 25) as a vibrational state preparation technique, we have explored the spectroscopy of the ν_1 N–H stretch[8] and the ν_3 and ν_2 N–C–O symmetric and antisymmetric stretch fundamentals.[26,27] In this paper, we describe the excitation from initially selected vibrational levels to the S_1 state that dissociates to produce selected quantum states of the fragments in dissociation channels (1) and (2). Previously,[8,26] we recorded HNCO Raman spectra by two methods, photoacoustic Raman spectroscopy (PARS) (Ref. 28) and action spectroscopy. The latter is a photodissociation experiment in which the Stokes laser in the SRE step scans through rovibrational transitions at fixed photolysis and probe laser wavelengths. Figure 1 is an energy level diagram that shows the vibrational and electronic excitation steps, the dissociation channels and their energies, and the laser induced fluorescence (LIF) interrogation of NCO ($X\ ^2\Pi$) and NH ($a\ ^1\Delta$).

Figure 2 presents the PAR spectra of the two most intense Raman transitions in HNCO, the ν_1 N–H stretch and the ν_3 N–C–O symmetric stretch fundamentals. The ground electronic state is a near prolate symmetric top with a large A rotational constant (more than 30 cm^{-1}).[18,29,30] The intense bands in the PAR spectra are ^QQ_K bands with well resolved K (Fig. 2 uses the asymmetric rotor notation, K_a) and unre-

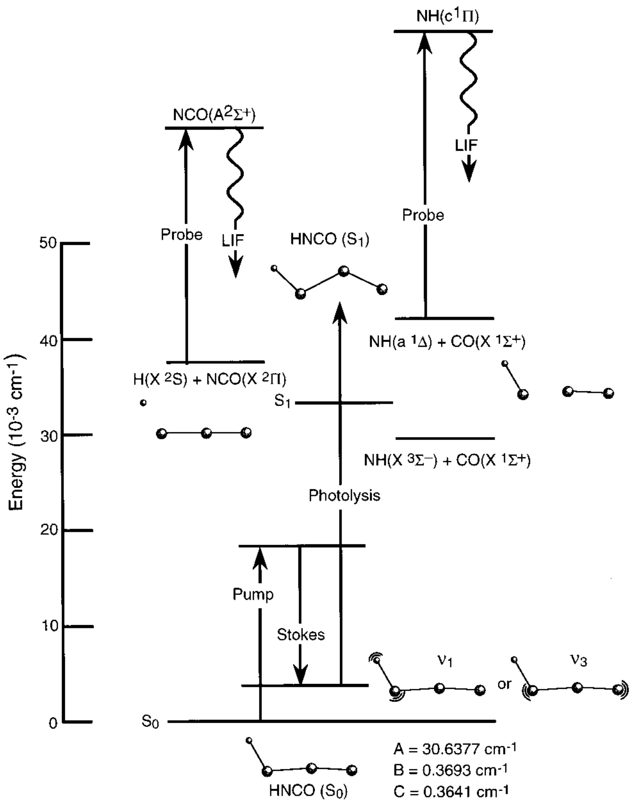

FIG. 1. Energy level diagram showing the Raman and electronic excitation, photodissociation pathways and LIF detection schemes.

solved J structure. The PAR spectra are highly irregular because of numerous perturbations of the vibrationally excited states. The N–C–O symmetric stretch mixes with several combination states containing two quanta of bend.[26] There are a number of combination bands that perturb the ν_1 spectrum, each consisting of a quantum of either ν_2 or ν_3, the N–C–O antisymmetric or symmetric stretch, and several quanta of bending excitation (ν_4, ν_5 or ν_6, the HNC bend, the NCO bend and the out-of-plane bend, respectively).[8] The perturbations shift the energy origins of the K_a sublevels unpredictably and alter the effective b-axis rotational constant $[\bar{B}=(B+C)/2]$ in the vibrationally excited states, making the shading of the unresolved J lines in the Raman Q-branch profiles irregular as well.

Many of the bands in the ν_1 and ν_3 PARS are previously unobserved and, hence, unassigned. We have used a simple rotational constant analysis based on the degree and the sign of the Q-branch shading to suggest which vibrational states are likely perturbers.[8] For example, in the ν_1 spectrum, the states labeled ν_α and ν_β have the form $(001v_4v_5v_6)$ where $v_4+v_5+v_6=3$. The state ν_γ may have the same form or may be made up of five quanta of bend, and the ν_x state, which splits the ν_1 $K_a=2$ band into a pair of transitions whose infrared absorptions are well characterized, is most likely (010110).[29,31] Although some of these previously unobserved bands are quite weak in the photoacoustic spectrum, their intensities in the action spectra are comparable to the other bands because they have good Franck–Condon factors in the electronic transition to the bent N–C–O geometry in S_1. Here we assign rotational quantum numbers (K_a) to the previously unobserved bands in the ν_1 spectrum, ν_α, ν_β and ν_γ, and to the bands in the ν_3 region of the Raman spectrum by observation of the structure in the electronic transitions out of states prepared by SRE. Scanning the photolysis laser at fixed Stokes and probe laser wavelengths (see Fig. 1) produces a photofragment yield spectrum. In addition to providing rotational assignments, photofragment yield spectroscopy measures resonance widths in the transition to the dissociative electronic state. Because the initial Raman state selection prepares a well-defined rovibrational level, it removes thermal congestion in the electronic excitation step and provides greater resolution than the room temperature ultraviolet absorption spectrum of HNCO reported by Dixon and Kirby.[20] Recent photofragment yield spectroscopy by Reisler and co-workers[10,15,17] of NH (a $^1\Delta$), NCO (X $^2\Pi$), and NH (X $^3\Sigma^-$) from supersonically cooled HNCO also removes thermal congestion in the $S_1 \leftarrow S_0$ transition. The molecular beam experiment further has the potential to provide vibrational assignments[24] since the photolysis laser may scan over an arbitrary frequency range without background from photolysis of thermally populated states. Despite its more limited frequency range, the SRE initial state prepara-

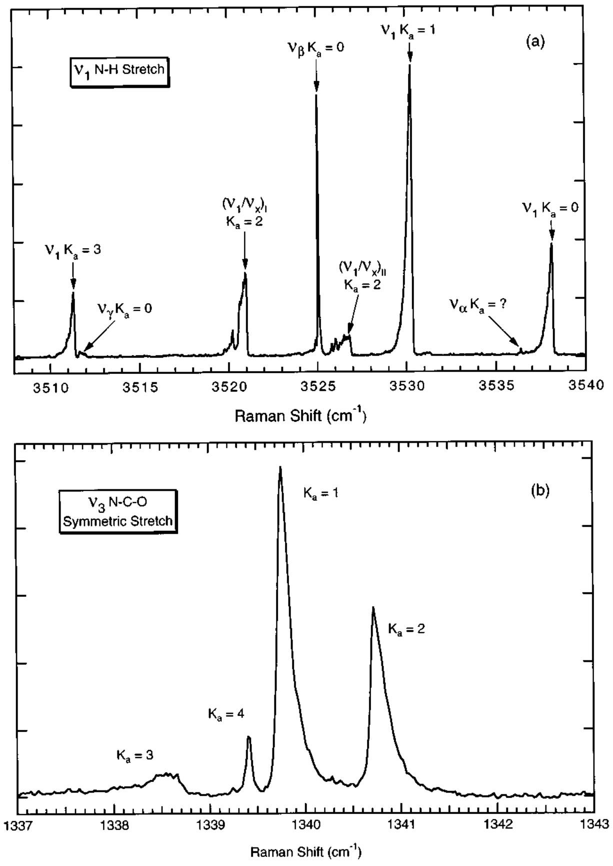

FIG. 2. Photoacoustic Raman spectra (PARS) of the ν_1 N–H stretch (a) and ν_3 N–C–O symmetric stretch (b) fundamental transitions in HNCO. The assignments for the K_a quantum number appear over each Q branch. In the ν_1 spectrum the assignments for perturbed vibrational states also appear.

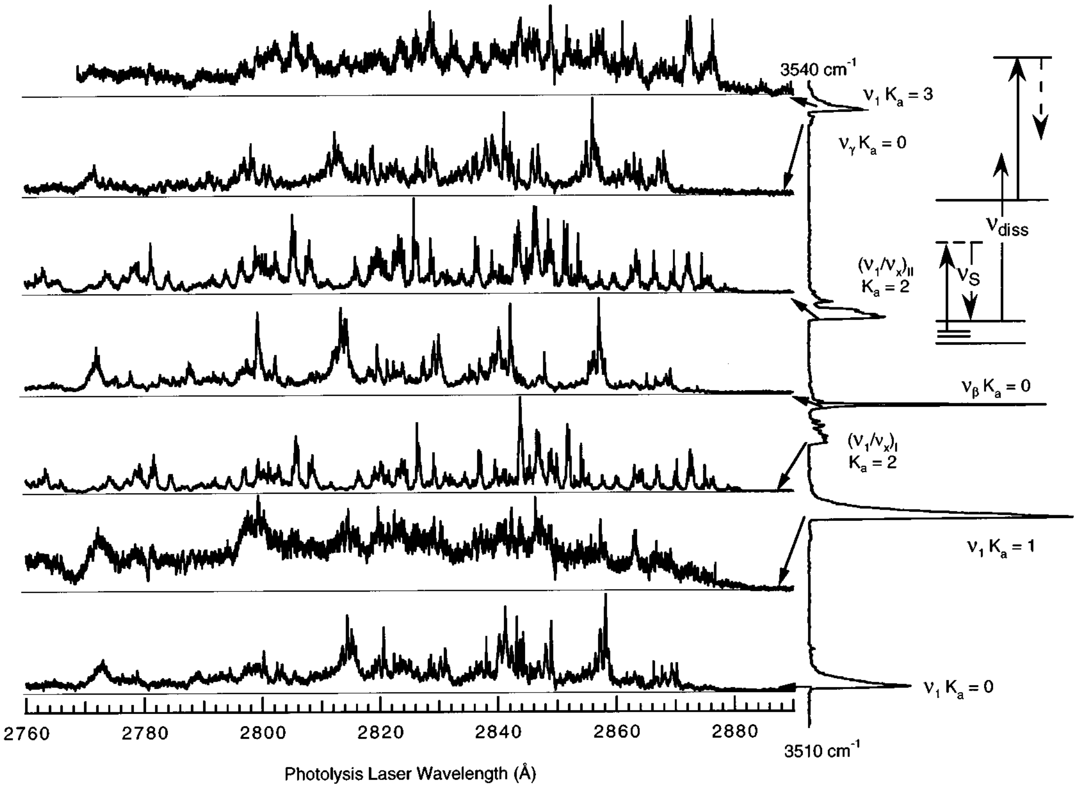

FIG. 3. NCO (X $^2\Pi$) photofragment yield spectra out of each of the K_a sublevels in the ν_1 manifold. The vertically plotted ν_1 PARS illustrates the initial state selection.

tion experiments described in this work have the advantage of exciting a variety of different initial rovibrational states, in particular the widely separated K_a energy levels in HNCO.

II. EXPERIMENTAL APPROACH

We have detailed the experimental approach elsewhere[7,8,27] and provide only a brief description here. The experiment requires four laser light sources: two to carry out the Raman excitation, one to photolyze vibrationally excited states prepared by SRE, and one to probe fragments by LIF. The fixed frequency pump light for the SRE is a fraction of the second harmonic of an injection seeded Nd:YAG laser, and the tunable Stokes light comes from a dye laser pumped with the remaining light from the same Nd:YAG laser. The photolysis light is the frequency doubled output of another Nd:YAG laser pumped dye laser system. The LIF probe laser is a XeCl excimer laser pumped dye laser. For probing NCO by LIF on the (A $^2\Sigma^+ \leftarrow X$ $^2\Pi$) transition[32,33] we use the fundamental of the dye laser directly at wavelengths between 420–480 nm, and for probing the NH (c $^1\Pi \leftarrow a$ $^1\Delta$) transition[34] we frequency double the dye laser output to produce the necessary 324–330 nm light. We align all four beams on the axis of a cylindrical, Pyrex cell with quartz windows mounted at Brewster's angle. The cell is equipped with a microphone for photoacoustic measurements and a quartz viewing window with an f/1 optical system and a photomultiplier tube (PMT) for collecting fluorescence signals. We synthesize isocyanic acid by the reaction of a saturated KOCN solution with concentrated phosphoric acid,[35] as described previously.[36] The HNCO vapor flows from a −78 °C reservoir of the liquid [vapor pressure on the order of 1 Torr (Ref. 37)] through the fluorescence cell, where its temperature and pressure are approximately 25 °C and 0.1 Torr.

III. RESULTS AND DISCUSSION

A. The H+NCO (X $^2\Pi$) channel

Figure 3 shows the NCO (000) photofragment yield curves from several different K_a sublevels in the ν_1, N–H stretch state. On the right side, plotted vertically, is the photoacoustic Raman spectrum, and on the left side, plotted horizontally, are the photolysis yield spectra for the initial states prepared by the Raman excitation. The spectral range includes the approximately 3000 cm^{-1} between the appearance threshold for the NCO fragment from photolysis of the ν_1 states and the onset of background signal due to photolysis of thermally populated states. Any vertical cut through the photolysis yield curves in Fig. 3 gives an action spectrum at a specific photolysis wavelength. The spectra of electronic transitions out of the vibrational states in the ν_1 manifold are highly structured, indicating a long-lived electronically excited state, and the structure varies considerably because of rotational resonances for different K_a states and different Franck–Condon factors for the distinct vibrational states. The presence of well-defined structure with resolved rota-

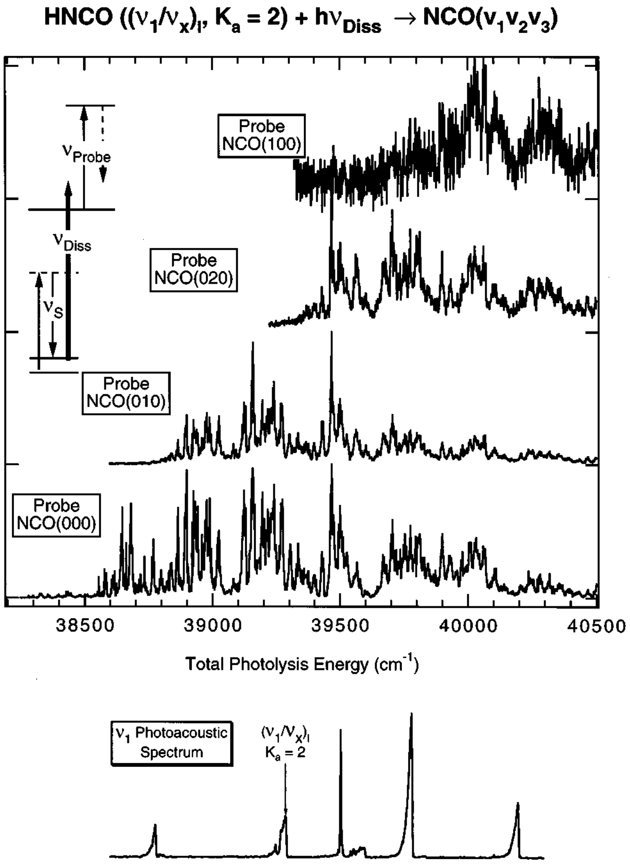

FIG. 4. NCO ($X\ ^2\Pi$) photofragment yield spectra originating in the $(\nu_1/\nu_x)_I$ $K_a=2$ level in HNCO and probing different vibrational levels in the NCO fragment. The abscissa is the total photolysis energy, or the sum of the photolysis photon energy and the Raman shift for the initial vibrational excitation. The ν_1 PARS plotted beneath the graph shows the initial state selection.

tional transitions is the key to the assignment of K_a values to the previously unobserved vibrationally excited states, ν_α, ν_β, and ν_γ.

1. Final state of NCO fragment

The NCO photofragment yield spectra in Fig. 3 have the LIF probe laser fixed on the Q_1 bandhead corresponding to the lower ($^2\Pi_{1/2}$) spin–orbit level of the vibrationless electronic ground state in the $A\ ^2\Sigma^+(000) \leftarrow X\ ^2\Pi(000)$ transition.[32,33] The experiment cleanly resolves the final vibronic NCO state but not the final rotational state because it probes a bandhead that includes approximately the lowest fifteen J states under the bandwidth of the probe laser.[38] Because of its complex vibronic energy level structure,[38,39] the NCO fragment presents many states to interrogate. Combined with the choice of the initial HNCO vibrational state, the choice of the final NCO state creates a matrix of possible state-to-state photofragment yield spectra. As Fig. 4 shows, however, the final NCO state has little influence on the resonances in the NCO yield spectrum. The initial state in all traces of Fig. 4 is the $(\nu_1/\nu_x)_I$ $K_a=2$ level (as indicated by the PAR spectrum at the bottom of the figure), but the probe laser is fixed to interrogate a different NCO vibrational level, in each case using the Q_1 bandhead of the lower spin-orbit state of the unique $K=\nu_2+1$ state.[33,39] All four traces have an identical set of resonances, with the most important difference among spectra probing higher NCO vibrational states being the energy shift of the appearance threshold. The dissociation from a bent NCO group in the S_1 state of HNCO to a linear NCO fragment preferentially populates excited bending states in NCO,[40,41] (where ν_2 is the degenerate bend) as shown by the relatively poor signal to noise ratio obtained probing NCO (100) (where ν_1 is the symmetric stretch).

2. Vibrational progressions in the $S_1 \leftarrow S_0$ transition

Dixon and Kirby[20] observed several vibrational progressions in the ultraviolet absorption spectrum of HNCO vapor at room temperature, but they did not assign the transitions to specific vibrational modes in the upper state. Their progressions, labeled A, B, C, and D, all had a characteristic spacing of approximately 500–600 cm^{-1}, consistent with excitation of a bending vibration in S_1. The most likely candidate is the NCO bend (ν_5 in S_0), whose experimentally measured frequency in S_0 is 577.4 cm^{-1} (Ref. 42) and whose calculated frequency in S_1 is very nearly the same.[23,27] Dixon and Kirby suggested that the presence of several similarly spaced progressions could be the result of transitions to both *cis* and *trans* isomers in S_1. *Ab initio* calculations of the S_1 surface do indeed show the presence of *cis* and *trans* minima and a substantial barrier to isomerization. The slightly bent NCO angle (172°) (Ref. 18) in S_0 places the Franck–Condon point closer to the *trans* isomer than to the *cis*.[13] Recent electronic absorption spectra of HNCO cooled in a supersonic jet show that there is only a single important progression with a spacing consistent with the NCO bending frequency.[10,24] The electronic absorption from vibrationally excited levels in S_0, particularly those that contain some NCO bend character, may access either well on the S_1 surface and may thus give rise to additional bands.

Our initial state-selected NCO photofragment yield spectra resolve rotational and vibrational progressions more cleanly than the room temperature absorption spectrum but still show numerous anomalies. The same type of vibrational state mixing that is prevalent in the ground electronic state of HNCO (Refs. 29, 43) probably contributes to the vibrational energy level structure in S_1, giving rise to the irregular vibrational progressions that we observe. In addition, although our Raman excitation prepares a single initial vibrational state and K_a rotational level, it populates a range of J states because we use Q-branch excitation. The electronic excitation spectra therefore have some rotational congestion. As Table I illustrates, we find two dominant progressions that are consistent with the C and D progressions of Dixon and Kirby. (The A and B progressions lie primarily below the NCO production threshold.) We are also able to resolve many other transitions that do not fall into a regular progression. Table II lists rotational assignments (described below) for the observed bands that correspond most nearly to the C and D bands since the vibrational spacing in these progres-

TABLE I. Vibrational progression in NCO photolysis yield spectra.

C Progression				*D* Progression				*E* Progression	
Dixon and Kirby		This work		Dixon and Kirby		This work		This work	
ν (cm^{-1})	$\Delta\nu$	ν (cm^{-1})	$\Delta\nu$	ν (cm^{-1})	$\Delta\nu$	ν (cm^{-1})	$\Delta\nu$	ν (cm^{-1})	$\Delta\nu$
38 174[a]				37 938				38 312.8	
	556				543				538.1
38 730		38 699.7		38 481		38 515.4		38 850.9	
	549		538.8		535		543.6		536.1
39 279		39 238.5		39 016		39 059.0		39 387.0	
	546		546.3		535		530.3		523.2
39 825		39 784.8		39 551		39 589.3		39 910.2	
	541		549		542		535.0		524
40 366		40 334		40 093		40 124.3		40 434	
	539				531				
40 905				40 629					

[a] Measurement from ${}^{R}Q_0$ in the UV spectrum (Ref. 20). All other measurements in Dixon and Kirby's work are band maxima. All measurements from this work are ${}^{R}Q_0$.

sions is relatively regular and approximately matches that of Dixon and Kirby.[20] There is one additional set of bands with a regular spacing consistent with NCO bend excitation that we arbitrarily label as E in Tables I and II. The energy range over which we may scan the NCO photofragment yield spectra is limited to the approximately 3000 cm^{-1} between the NCO appearance threshold and the onset of significant background signal due to photolysis of thermally populated states. This limited range precludes the assignment of bands to excitation of specific vibrational levels in the upper state.

3. Initial rotations

The rotational structure within each vibrational band results from the initial K_a quantum number selected in the SRE step. The electronic absorption is a perpendicular transition with prolate top selection rules of $\Delta K = \pm 1$, $\Delta J = 0, \pm 1$, and the bent N–C–O angle in S_1 leads to a large decrease in the A rotational constant, $\Delta A = -26\ \mathrm{cm}^{-1}$.[20] The prolate top rotational energy levels are $E(J,K) = A_{\mathrm{eff}}\ K^2 + \overline{B}J(J+1)$,[44] where $A_{\mathrm{eff}} = A - \overline{B}$ and $\overline{B} = (B+C)/2$, and the large ΔA separates rotational transitions for different initial values of K_a by up to several hundred wave numbers. Table III lists the anticipated line positions and splittings for ${}^{P,R}Q_K$ (prolate top notation ${}^{\Delta K}\Delta J_K$) branch transitions relative to ${}^{R}Q_0$ based on the K_a rotational energy levels for S_0 (Refs. 18, 29, 30) and the best fit values of A_{eff} in S_1 from this work. In NCO yield spectra originating in $K_a = 0$, there is a single Q branch (${}^{R}Q_0$) for each vibrational transition, while for $K_a > 0$ the Q branches occur in pairs (${}^{R}Q_K, {}^{P}Q_K$) that are progressively more red-shifted and have larger splitting with increasing

TABLE II. Line positions (cm^{-1}) for $K_a'' = 0-4$ in the NCO photolysis yield spectrum.

Band	${}^{R}Q_0$	${}^{P}Q_1$	${}^{R}Q_1$	${}^{P}Q_2$	${}^{R}Q_2$	${}^{P}Q_3$	${}^{R}Q_3$	${}^{P}Q_4$	${}^{R}Q_4$
E	38 312.8	38 281.9	38 296.8						
D	515.4	481.8	495.6	397.7	427.0	267.1	311.1	38 092.2	151.2
C	699.7	665.9	682.5	583.5[a]	616.1	451.7	obscured	281.5	339.3
C	723.7	691.3	704.8	604.9	635.0	474.2	obscured	300.3	353.9
C	763.3	730.2	745.1	645.5	678.6	515.2	567.3	339.3	obscured
E	850.9	818.0	832.5	732.9	761.4	602.0	646.5	425.3	obscured
D	39 059.0	39 026.0	39 040.2	940.4	970.1	808.9	854.8	635.9	696.6
C	199.8			39 082.2	obscured				
C	238.5			121.8	39 152.8			818.1	881.1
C	262.3			145.2	obscured				
E	387.0			270.6	302.6				
D	589.3			466.3	498.8				
C	784.8			670.5	701.6				
E	910.2			794.5	824.8				
D	40 124.3			40 008.5	40 039.1				
C	334			208	242				
E	434			316	354				
		$K_a''=1$		$K_a''=2$		$K_a''=3$		$K_a''=4$	
Avg $P-R$ splitting		14.2±1.1		30.4±1.7		45.1±1.1		58.5±2.9	
Average A_{eff}'		3.6±0.3		3.8±0.2		3.8±0.1		3.7±0.2	

[a] Indicates weak transition.

TABLE III. Calculated line positions and splittings (cm^{-1}) for $K''>0$.

K''	$E(K'')$[a]	$E(K')$[b]	Position relative to $^RQ_0$ ^PQ_K	^RQ_K	^PQ_K-^RQ_K Splitting[c]
1	30.1	3.7	−33.8	−19.0	14.8
2	118.4	14.8	−118.4	−88.8	29.6
3	260.6	33.3	−249.5	−205.1	44.4
4	452.3	59.2	−422.7	−363.5	59.2

[a] $E(K'')$ from infrared measurements, Ref. 30.
[b] $E(K')=A_{\mathrm{eff}}K^2$; $A_{\mathrm{eff}}=(A-\bar{B})$; $\bar{B}=(B+C)/2$.
[c] $\nu_R-\nu_P=4K''A'_{\mathrm{eff}}$.

K_a. Because SRE excites a range of J states in the initial state preparation, spectral overlap in the electronic transition makes the Q branch transitions the most intense.

Figure 5 presents NCO (000) photolysis yield spectra from three separate initial states in the ν_1 manifold, all of which have the same set of resonances when plotted against a scale of total photolysis energy (Raman shift plus photolysis photon energy). The lower trace originates in the ν_1, $K_a=0$ pure stretch state, and the similarity of the electronic spectra going through the previously unobserved states, ν_β and ν_γ, in the upper two traces allows a confident assignment of rotational quantum number $K_a=0$ to these states as well. In a similar fashion, we have assigned the K_a quantum number to several previously unidentified bands in the Raman spectra of both the N–H stretch (ν_1) (Ref. 8) and the N–C–O symmetric stretch (ν_3) (Ref. 26) regions. The characteristic splitting of bands in the electronic transition results directly from the initially selected K_a state, as shown in Table III.

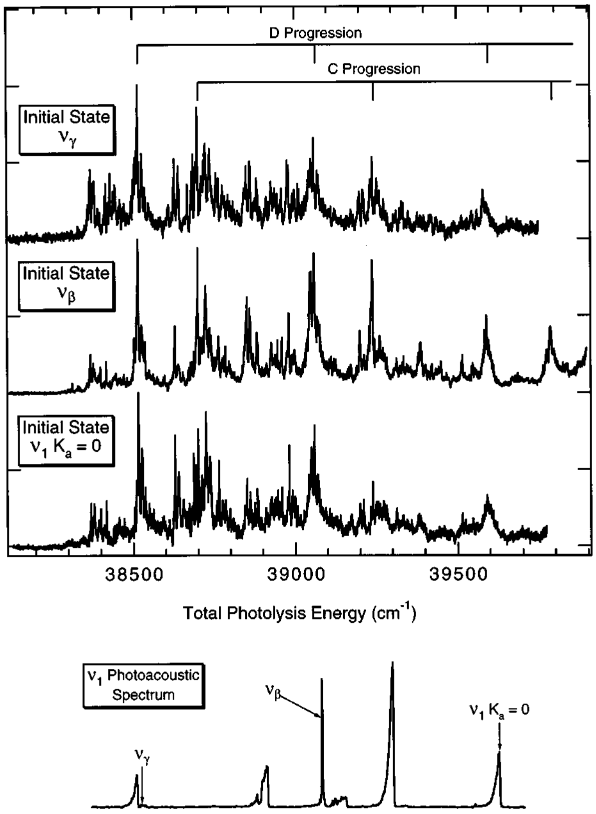

FIG. 5. NCO (X $^2\Pi$) photofragment yield spectra originating in three different vibrational states within the ν_1 manifold and probing NCO in the (000) vibrational state. The ν_1 PARS plotted beneath the graph shows the three different initial states, which are the combination states, ν_β and ν_γ, and the N–H stretch state, ν_1 $K_a=0$.

The comb at the top of Fig. 5 marks our identification of the $^RQ_0$ line positions belonging to Dixon and Kirby's C and D progressions. Our line positions differ from theirs because they identified overall vibrational band maxima without rotational resolution in this region of the spectrum, whereas the double resonance experiment isolates $^RQ_0$ more clearly (see Table I). There are numerous transitions in Fig. 5 to vibrational states not belonging to the C or D progressions, and even the bands in the C progression itself appear to be split into a series of three distinct transitions, as Table II illustrates. The most complete set of data in Table II is for lines that originate in $K_a=0$ and 2. As described further below, because the structure in the ν_1 $K_a=1$ NCO photolysis yield spectrum is too diffuse to identify any lines, the $K_a=1$ data in Table II come from initial preparation of ν_3 $K_a=1$, which has a lower vibrational frequency and thus a smaller range over which we may scan the NCO yield spectrum without significant single-photon dissociation of thermally populated states. The $K_a=3$ and 4 data come from initial excitation of both ν_1 and ν_3 states, but the rotational populations are small for these levels and the lines are more difficult to discern, especially in the more diffuse, higher energy region of the spectrum.

Table II also presents the average splitting between ^RQ_K and ^PQ_K bands and the corresponding value of A'_{eff}, which directly determines the $P-R$ splittings for the $K''_a>0$ transitions (see Table III). There is considerable variation in the $P-R$ splittings in Table II that reflects both the difficulty in locating the exact position of the peaks of the Q-branch transitions in our spectra and possibly also the different rotational constants for different vibrational states in S_1. The average excited state rotational constant from our data is $A'_{\mathrm{eff}}=3.7\pm0.2$ cm^{-1}, close to Dixon and Kirby's value of $A'_{\mathrm{eff}}=4$ cm^{-1}.[20]

4. Initial vibrations

The character of the initial vibrational state affects the structure in the transition to S_1 by influencing the dissociation mechanism or dynamics and, therefore, the lifetime of the excited electronic state. A clear example appears in the NCO photofragment yield spectra of the ν_1 $K_a=1$ and $K_a=3$ states. Figure 3 shows that there is clearly resolved rotational structure in the NCO yield spectrum of every initial rovibrational state in the ν_1 manifold except for $K_a=1$. The $K_a=3$ state has some structure in its NCO yield spectrum, but also a large component of diffuse background. As noted above, the $K_a=1$ spectrum is so diffuse that it cannot be used to assign a K_a quantum number to the initial state (the rotational assignment for ν_1 $K_a=1$ comes from infrared spectroscopy[29]). The vibrationally excited states of HNCO tend to be perturbed by interactions that depend quite strongly on the value of K_a, but the $K_a=1$ and 3 levels are unmixed, pure N–H stretch states.[8,29] The other K_a sublevels in the ν_1 manifold are mixed by varying amounts with background states that contain several quanta of bending excitation. The mixed N–H stretch–bending states have favorable Franck–Condon factors to reach S_1 compared to the unperturbed N–H stretch states, as evidenced by the poor signal to noise ratio in the ν_1 $K_a=1$ NCO photofragment yield spectrum of Fig. 3.

The overlap between vibrational states in S_1 and different initially prepared vibrational states in S_0 may be the key to understanding the influence of initial vibrational states on the resonance widths. There appear to be two sets of resonances in all of the NCO yield spectra in Fig. 3, one of which is structured and tends to be quite strong, and a second, much weaker, broad continuum. The perturbed ν_1 states have strong transitions to the structured bands but also show weak transitions to the continuum. The unperturbed ν_1 levels only have good overlap with the latter. We suggest that the structured bands are transitions to vibrational levels in S_1 that have excitation in the NCO bend or other coordinates that improve the Franck–Condon factor with the ground state, and that the continuous absorption excites states that have N–H stretch excitation in S_1. The latter have shorter lifetimes and broad resonances. We have shown elsewhere[23] that initial vibrational excitation of the N–H bond leads to preferential Franck–Condon overlap with states in S_1 that have N–H stretch excitation. The N–H bond length and frequency do not change significantly between S_0 and S_1, and, consequently, the diagonal transitions in the ν_1 vibration are more than ten times stronger than the off-diagonal transitions. The states that perturb the ν_1 fundamental have no N–H stretch excitation but significant NCO stretch and bend excitation, and they contribute more strongly to the overall Franck–Condon factors of the mixed states. Thus, the background state character dominates the Franck–Condon factors of the mixed states, and those states overlap primarily with states in S_1 that have no N–H stretch excitation.

There are two likely explanations for the broad resonances to S_1. Depending on the size and width of the barrier to N–H dissociation on the excited surface, N–H stretch excitation may increase the tunneling rate and lead to a direct dissociation on S_1 and a consequent reduction in the lifetime. A recent calculation of the barrier height suggests that, at least for energies near the dissociation threshold, this mechanism is unlikely. The two isomers in S_1 (*cis* and *trans*) have comparable minimum energies, but the barrier to dissociation from the *trans* well is about 8800 cm^{-1} above the H+NCO asymptote, while the barrier from the *cis* well is 4500 cm^{-1}.[13] Even for a hydrogen atom, the tunneling probability across either barrier is too small at threshold to compete with internal conversion to S_0.[45] However, at energies closer to the top of the barriers, the tunneling rate may become comparable to the internal conversion rate, and the initial vibrational level may influence the competition between direct and indirect dissociation.

The most likely explanation for the broad resonances is an increase in the crossing rate to S_0 from states that have N–H stretch excitation in S_1. The S_0 and S_1 surfaces do not intersect,[13] but in the N–H bond coordinate their closest approach must lie along the inner repulsive walls since the S_1 surface goes through a barrier at long N–H bond lengths while S_0 does not. Vibrational states with one or more quanta of ν_1 may have better overlap with high vibrational levels on S_0 at the inner turning point of the N–H oscillator. Zyrianov *et al.*[17] used similar reasoning to explain a lack of structure in the NH (X $^3\Sigma^-$) photofragment yield spectrum above the NH (a $^1\Delta$) production threshold, postulating that the crossing from S_1 to T_1 that leads to dissociation in the triplet channel is most favorable at the Franck–Condon point on S_1. Regardless of the mechanism, the important point is that direct vibrational excitation of the N–H dissociation coordinate on S_0 leads to a shorter lifetime in S_1 and, thus, a broader set of resonances in the electronic transition.

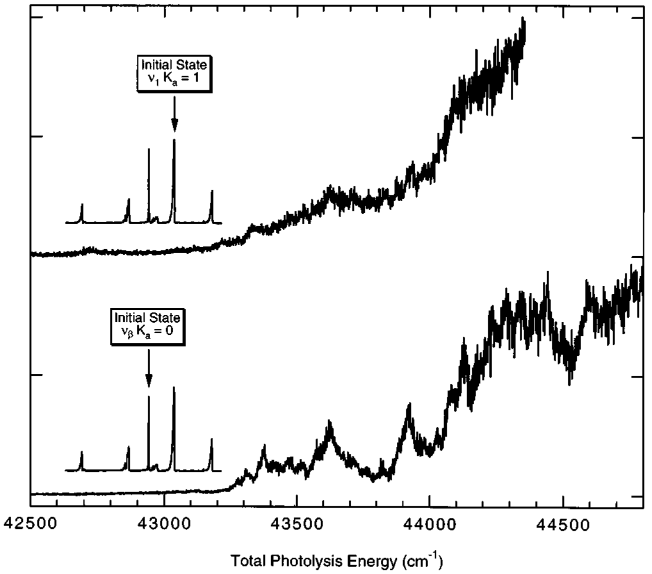

FIG. 6. NH (a $^1\Delta$) photofragment yield spectra originating in two different vibrational and rotational states in the ν_1 manifold and probing NH on the $Q(2)$ line of the (c $^1\Pi \leftarrow a$ $^1\Delta$) transition. The ν_1 PARS in the insets of each graph indicate the initial state selection of either the unperturbed ν_1 $K_a=1$ state or the perturbing ν_β $K_a=0$ state.

B. The NH (a $^1\Delta$)+CO channel

The photofragment yield spectra probing the NH (a $^1\Delta$) fragment are qualitatively different from the NCO yield spectra in that they are more diffuse and do not display well-defined resonances that depend on the initially selected rotational state. The threshold for spin-allowed cleavage of the C–N bond lies significantly higher in energy,[7,10] and above the NH (a $^1\Delta$)+CO threshold direct dissociation on the S_1 surface competes with crossing to S_0.[11,14,16,46] Figure 6 displays NH (a $^1\Delta$) photolysis yield spectra for two different initially selected states in the ν_1 manifold, ν_β, which has mostly background vibrational state character, and the ν_1 $K_a=1$ unperturbed N–H stretch state. The former shows coarse vibrational structure, consistent with previous observations of the features in the NH (a $^1\Delta$) photofragment yield spectrum from HNCO cooled in a molecular beam.[10] The latter, however, is relatively unstructured, indicating that an absorption to a continuous background dominates the NH ($a\ ^1\Delta$) yield spectrum of the unperturbed N–H stretch states in a fashion similar to the NCO yield spectra. The broadening of the NH ($a\ ^1\Delta$) yield resonances, which probe dissociation of the C–N bond, probably reflect a decrease in the S_1 lifetime due to dissociation of the N–H bond or crossing to S_0 that is influenced by vibrational excitation of the N–H coordinate. The NH ($a\ ^1\Delta$) production threshold lies at approximately the same energy as the top of the barrier for N–H dissociation from the *cis* well on S_1 and about halfway to the top of the barrier for dissociation from the *trans* well.[7,10,13] Therefore, it is possible that a direct dissociation of the N–H bond competes with the direct C–N bond fission on S_1 to give the continuous absorption.

IV. SUMMARY

Photofragment yield spectroscopy is a state-to-state electronic absorption measurement from a well-defined, initially selected vibrational and rotational level in the ground electronic state into a particular dissociation channel and fragment quantum state. We use SRE to prepare selected K_a sublevels in either the ν_1 N–H stretch or ν_3 N–C–O symmetric stretch fundamentals of HNCO. Both vibrational levels are strongly perturbed, and each K_a sublevel has a different vibrational character as a result of state mixing. We detect N–H or C–N bond fissions by LIF of the NCO ($X\ ^2\Pi$) or NH ($a\ ^1\Delta$) fragments, respectively. Near the N–H dissociation threshold, the NCO photofragment yield spectra show rotational and vibrational resonances that correspond roughly to those established previously from the room temperature absorption spectrum,[20] although the double resonance experiment is better able to resolve band origins. The form of the resonances is invariant to the final state of NCO but depends strongly on the initial state of the HNCO molecule. Selection of the initial K_a rotational state gives rise to a set of resonances in the electronic transition that allow assignment of K_a to previously unidentified, perturbed vibrational states in both the ν_1 and ν_3 manifolds. In addition, the character of the initial vibrational state influences the manifold of resonances to which there is favorable Franck–Condon overlap in the electronic excitation step. The unperturbed, excited N–H stretch states have transitions to a weak, continuous absorption that probably corresponds to states with N–H stretch excitation in S_1. These states dissociate more rapidly, most likely because of an increase in the coupling to S_0. The NH ($a\ ^1\Delta$) photofragment yield spectra display more diffuse resonances with no resolvable rotational structure because the threshold for this channel lies higher in energy and the dissociation mechanism is direct. The unperturbed ν_1 levels in S_0 give rise to a diffuse, unstructured NH ($a\ ^1\Delta$) yield spectrum, probably as a result of the decrease in the S_1 lifetime due to excitation of the N–H dissociation coordinate.

ACKNOWLEDGMENTS

We thank the Division of Chemical Sciences of the Office of Basic Energy Sciences of the Department of Energy for supporting this work. We also thank Professors Hanna Reisler and Reinhard Schinke for useful discussions and for sharing their results in advance of publication.

[1] (a) F. F. Crim, Annu. Rev. Phys. Chem. **44**, 397 (1993); (b) R. L. Vander Wal, J. L. Scott, F. F. Crim, K. Weide, and R. Schinke, J. Chem. Phys. **94**, 3548 (1991); (c) R. L. Vander Wal, J. L. Scott, and F. F. Crim, *ibid.* **94**, 1859 (1991).

[2] (a) I. Bar, Y. Cohen, D. David, T. Arusi-Parpar, S. Rosenwaks, and J. J. Valentini, J. Chem. Phys. **95**, 3341 (1991); (b) D. David, A. Strugano, I. Bar, and S. Rosenwaks, *ibid.* **98**, 409 (1993); (c) Y. Cohen, I. Bar, and S. Rosenwaks, *ibid.* **102**, 3612 (1995).

[3] J. Zhang, C. W. Riehn, M. Dulligan, and C. Wittig, J. Chem. Phys. **103**, 6815 (1995).

[4] M. Brouard and S. R. Langford, J. Chem. Phys. **106**, 6354 (1997).

[5] H. T. Liou, K. L. Huang, and M. C. Chen, Chem. Phys. Lett. **266**, 591 (1997).

[6] S. S. Brown, R. B. Metz, H. L. Berghout, and F. F. Crim, J. Chem. Phys. **105**, 6293 (1996).

[7] S. S. Brown, H. L. Berghout, and F. F. Crim, J. Chem. Phys. **105**, 8103 (1996).

[8] S. S. Brown, H. L. Berghout, and F. F. Crim, J. Chem. Phys. **106**, 5805 (1997).

[9] H. Okabe, J. Chem. Phys. **53**, 3507 (1970).

[10] M. Zyrianov, T. Droz-Georget, A. Sanov, and H. Reisler, J. Chem. Phys. **105**, 8111 (1996).

[11] T. Droz-Georget, M. Zyrianov, H. Reisler, and D. W. Chandler, Chem. Phys. Lett. **276**, 316 (1997).

[12] C. R. Brazier, R. S. Ram, and P. F. Bernath, J. Mol. Spectrosc. **120**, 381 (1986).

[13] J. Klossika, H. Flöthmann, C. Beck, R. Schinke, and K. Yamashita, Chem. Phys. Lett. **276**, 325 (1997).

[14] M. Kawasaki, Y. Sato, K. Suto, Y. Matsumi, and S. H. S. Wison, Chem. Phys. Lett. **251**, 67 (1996).

[15] T. Droz-Georget, M. Zyrianov, A. Sanov, and H. Reisler, Ber. Bunsenges. Phys. Chem. **101**, 469 (1997).

[16] A. Sanov, T. Droz-Georget, M. Zyrianov, and H. Reisler, J. Chem. Phys. **106**, 7013 (1997).

[17] M. Zyrianov, T. Droz-Georget, and H. Reisler, J. Chem. Phys. **106**, 7454 (1997).

[18] K. Yamada, J. Mol. Spectrosc. **79**, 323 (1980).

[19] A. L. L. East, C. S. Johnson, and W. D. Allen, J. Chem. Phys. **98**, 1299 (1993).

[20] R. N. Dixon and G. H. Kirby, Trans. Faraday Soc. **64**, 2002 (1968).

[21] J. W. Rabalais, J. M. McDonald, V. Scherr, and S. P. McGlynn, Chem. Rev. **71**, 73 (1971).

[22] W.-H. Fang, X.-Z. You, and Z. Yin, Chem. Phys. Lett. **238**, 236 (1995).

[23] S. S. Brown, C. M. Cheatum, D. Fitzwater, and F. F. Crim, J. Chem. Phys. **105**, 10 911 (1996).

[24] H. Reisler (private communication).

[25] (a) F. DeMartini and J. Ducuing, Phys. Rev. Lett. **17**, 117 (1966); (b) G. O. Sitz and R. L. Farrow, J. Chem. Phys. **93**, 7883 (1990); (c) D. A. V. Kliner, D. E. Adelman, and R. N. Zare, *ibid.* **95**, 1649 (1991); (d) K. Ravichandran, M. Yorgancioglu, and T. R. Fletcher, *ibid.* **101**, 3406 (1994).

[26] S. S. Brown, H. L. Berghout, and F. F. Crim, J. Chem. Phys. (in press).

[27] S. S. L. Brown, Ph.D. thesis, University of Wisconsin-Madison, 1996.

[28] J. J. Barrett, in *Chemical Applications of Nonlinear Raman Spectroscopy*, edited by A. B. Harvey (Academic, New York, 1981), pp. 89–169.

[29] K. M. T. Yamada, M. Winnewisser, and J. W. C. Johns, J. Mol. Spectrosc. **140**, 353 (1990).

[30] M. Niedenhoff, K. M. T. Yamada, and G. Winnewisser, J. Mol. Spectrosc. **176**, 342 (1996).

[31] J. H. Teles, G. Maier, B. A. J. Hess, L. J. Schaad, M. Winnewisser, and B. P. Winnewisser, Chem. Ber. **122**, 753 (1989).

[32] (a) T. R. Charlton, T. Okamura, and B. A. Thrush, Chem. Phys. Lett. **89**,

98 (1982); (b) R. A. Copeland and D. R. Crosley, Can. J. Phys. **62**, 1488 (1984).

[33] D. Patel-Misra, D. G. Sauder, and P. J. Dagdigian, J. Chem. Phys. **93**, 5448 (1990).

[34] (a) R. S. Ram and P. F. Bernath, J. Opt. Soc. Am. B **3**, 1170 (1986); (b) W. Ubachs, G. Meyer, J. J. Ter Meullen, and A. Dymanus, J. Mol. Spectrosc. **115**, 88 (1986); (c) B. Bohn, F. Stuhl, G. Parlant, P. J. Dagdigian, and D. R. Yarkony, J. Chem. Phys. **96**, 5059 (1992).

[35] R. A. Ashby and R. L. Werner, J. Mol. Spectrosc. **18**, 184 (1965).

[36] S. S. Brown, H. L. Berghout, and F. F. Crim, J. Chem. Phys. **102**, 8440 (1995).

[37] M. Linhard, Z. Anorg. Allg. Chem. **236**, 200 (1938).

[38] (a) R. N. Dixon, Philos. Trans. R. Soc. London, Ser. A **252**, 165 (1960); (b) P. S. H. Bolman, J. M. Browm, A. Carrington, I. Kopp, and D. A. Ramsay, Proc. R. Soc. London, Ser. A **343**, 17 (1975).

[39] J. T. Hougen, J. Chem. Phys. **36**, 519 (1961).

[40] J. Zhang, M. Dulligan, and C. Wittig, J. Phys. Chem. **99**, 7446 (1995).

[41] S. S. Brown, H. L. Berghout, and F. F. Crim, J. Phys. Chem. **100**, 7948 (1996).

[42] D. A. Steiner, K. A. Wishah, S. R. Polo, and T. K. McCubbin, J. Mol. Spectrosc. **76**, 341 (1979).

[43] B. P. Winnewisser, in *Molecular Spectroscopy; Modern Research*, edited by N. K. Rao (Academic, Orlando, Florida, 1985), pp. 321–419.

[44] I. N. Levine, *Molecular Spectroscopy* (Wiley, New York, 1975).

[45] T. Baer and W. L. Hase, in *Unimolecular Reaction Dynamics* (Oxford University Press, New York, 1996), pp. 264–266.

[46] (a) W. S. Drozdoski, A. P. Baronovski, and J. R. McDonald, Chem. Phys. Lett. **64**, 421 (1979); (b) T. A. Spiglanin, R. A. Perry, and D. W. Chandler, J. Chem. Phys. **87**, 1568 (1987); (c) T. A. Spiglanin and D. W. Chandler, *ibid*. **87**, 1577 (1987); (d) B. Bohn and F. Stuhl, J. Phys. Chem. **97**, 4891 (1993).